Results in Physics 7 (2017) 1628–1633

Contents lists available at ScienceDirect

Results in Physics

journal homepage: www.journals.elsevier.com/results-in-physics

Characterization, preparation, and reaction mechanism of hemp stem based activated carbon

Ji Zhang [a], Jianmin Gao [a], Yao Chen [a,*], Xinmin Hao [b], Xiaojuan Jin [a]

[a] MOE Key Laboratory of Wooden Material Science and Application, Beijing Key Laboratory of Lignocellulosic Chemistry, MOE Engineering Research Centre of Forestry Biomass Materials and Bioenergy, Beijing Forestry University, 35 Qinghua East Road, Haidian, 100083 Beijing, China
[b] The Research Center of China-hemp Materials, The Quartermaster Research Institute of the General Logistics Department of the PLA, 28 Xizhimen North Street, 100088 Beijing, China

ARTICLE INFO

Article history:
Received 8 March 2017
Received in revised form 21 April 2017
Accepted 23 April 2017
Available online 26 April 2017

Keywords:
Hemp stem
Activated carbon
Characterization
Reaction mechanism

ABSTRACT

In this study, hemp stem was used to prepare high surface area activated carbon (AC) by KOH activation. The structure, characterization, thermal and structure analysis on reaction mechanisms of AC were investigated via N_2 adsorption–desorption isotherm, Fourier transform infrared (FTIR) spectroscopy and thermogravimetric-mass (TG-MS) spectrometry. Results show that when the impregnation ratio is 4.5:1 (KOH/char), the activation temperature is 800 °C, and the activation time is 1.5 h, AC has the highest specific surface area of 2388 $m^2 \cdot g^{-1}$ and exhibits narrow pore size distributions with maxima in the micropore areas. The reaction mechanism of AC from hemp stems by KOH activation is as follows: In the first carbonization stage, it is primarily because of the substitution, scission, and oxidization reactions of methylene. Then in the second activation stage, it is mainly related to polycyclic reactions, reactions between carbon and KOH, and reactions between intermediate potassium oxide species and carbon.

Introduction

Activated carbon (AC) which has flourishing hole structure and high adsorption capability is an important industrial material. And the properties of AC are also affected by the type of activator, the ratio of added activator, activation temperature, activation time and so on [1,2]. In consideration of activation difficulty, supply stability and the price of raw materials, AC can be prepared by a wide range of different raw materials [3]. The use of agriculture by-products or lignocellulosic materials, such as rice husks and waste newspapers to produce AC has been widely studied. Kazemipour et al. [4], respectively used some agricultural products such as almond, hazelnut, walnut, and apricot to prepare AC (specific surface area was between 635 $m^2 \cdot g^{-1}$and 1208 $m^2 \cdot g^{-1}$) Hemp, which can grow quickly in various climates and has various applications is an good choice owing to low cost, economic, and environmental considerations [5].

Hemp, an annual herbaceous plant, as a result of hemp fiber processing technology is rapidly expanding, is widely cultivated in China (the planting area is around 40 thousand hectare). However, compared to hemp seed can be refined into biological diesel and hemp bast can be applied in the clothing [6], respectively. The hemp stems are almost useless and ofen burned through post-harvest burning of cultivation fields, which not only wastes the resources, but also polluts the environment. Hemp stems are very rich in cellulose and lignin, and have natural nano pore structure. Accordingly, the utilization of hemp stems to produce AC reduce the cost, enhance economic efficiency and contribute to comprehensive utilization of agricultural wastes [7,8].

There are two processes for the preparation of activated carbons, the so-called physical and chemical activation. The results show that chemical activation has the advantage of high effective and well-controlle porosity. In spite of all kinds of activating agents are used, KOH which can promote AC to produce more pore structure is one of the most widely applied. Rosas et al. [9] adopted phosphoric acid activation to producet AC (specific surface area was 1500 $m^2 \cdot g^{-1}$) from hemp. A.H. Basta et al. [10] used 2-steps KOH activation to prepare AC (specific surface area was 1917 $m^2 \cdot g^{-1}$) from rice straw. However, straw-based material such as hemp stems often have high ash content compared with other agricultural wastes, which are not benefit for the preparation of super AC. As a consequence, preparation and characterization of high performance AC from straw material was studied by few researchers. Not to mention the preparation mechanisms of straws materials-derived AC were investigated. Only Ru Yang et al. investigated characterization of AC derived from biomass source hemp stem via N_2, CO_2 and H_2 adsorption [11].

* Corresponding author.
E-mail address: jmgao@bjfu.edu.cn (Y. Chen).

http://dx.doi.org/10.1016/j.rinp.2017.04.028
2211-3797/

In this study, hemp stem based AC which has high BET was prepared by KOH activation. Characterization of AC and several important factors about preparation such as impregnation ratio, activation temperature and activation time were investigated. Moreover, thermal and structure analysis about preparation mechanisms of AC were also studied via FTIR and TG-MS.

Materials and methods

Preparation of super activated carbon based on hemp stems

Hemp stem was collected from China's Yunnan as the carbon source. KOH, HCl, KBr and distilled water come from Beijing kebaiao biotechnology (Beijing, China) are all analytical grade.

In carbonization step, hemp stem was heated at a rate of 10 °C/min up to 500 °C and kept 1 h at this temperature in N_2 atmosphere. The samples after carbonization were ground. The particle samples were soaked in KOH solution of 50% concentration for 24 h, then were dried at 103 ± 2 °C for 12 h [12]. The mass ratio of KOH/samples was 3:1, 3.5:1, 4:1, 4.5:1, 5:1, 5.5:1 or 6:1, respectively. In activation step, the KOH-impregnated samples were heated at a rate of 10 °C/min up to the final temperature and kept some time at final temperature in N_2 atmosphere. The final temperature ranged from 700 to 900 °C, for example, 700, 750, 800, 850 and 900 °C. The activation time ranged from 0.5 to 2.5 h, for example, 0.5, 1, 1.5, and 2.5 h. Finally, these samples (AC) were repeatedly washed with hot distilled water until pH of the solution reached about 6–7, then were dried at 103 ± 2 °C for 12 h.

Characterization of hemp stem-based activated carbon

Nitrogen sorption isotherms were determined at 77 K with a Micromeritics ASAP 2020 sorption analyzer. The BET method was utilized to calculate the specific surface areas. The surface areas were measured by the BET calculation method according to the adsorption branch of the isotherms. The total pore volume was defined as the volume of liquid nitrogen, corresponding to the amount adsorbed at a relative pressure of $p/p_0 = 0.99$.

The chemical characterization of functional groups of the samples was investigated by the Fourier transform infrared spectrometer (Bruker, Tensor27) between 4000 and 400 cm^{-1} rang, adopting pellets with samples dispersed in KBr.

The simultaneous thermogravimetric-mass spectrometric (TG-MS) analysis of the samples were measured in a TG/DTA/DSC thermal analyzer (Setsys Evolution 16/18, Setaram) coupled to a mass spectrometer (Omni star, Pfeiffer). Samples were heated from 50 to 1000 °C at 10 °C/min in helium atmosphere (flow rate = 50 mL/min). Meanwhile, the weight loss was also calculated in this range. Simultaneously, gases were analyzed at time intervals of 0.2 s. Ions of m/z 2, 18, 28 and 44 were chosen to calculate the concentrations of H_2, H_2O, CO and CO_2, respectively.

Results and discussion

The effect of impregnation ratio

The analyses of the N_2 adsorption–desorption isotherms are calculated by applying the BET equation, t-plot and DFT methods. Yield and pore structure characteristic of hemp stems-based activated carbon (AC), such as surface areas, total pore volumes, micropore volume, average pore diameter are shown in Table 1, respectively.

When activation temperature is 800 °C and activation time is 1 h, the BET surface area of the AC is changed from 1849 to 2312 $m^2 \cdot g^{-1}$ with the variation of impregnation ratio. When the impregnation ratio is 3:1, there is little impregnated activation (KOH) to promote the formation of skeleton structure of carbon and the generation of pore structure, and the BET surface area was the lowest (1849 $m^2 \cdot g^{-1}$). With the increasing of impregnation ratio, the BET surface area raises significantly and reachs maximum (2312 $m^2 \cdot g^{-1}$) when the impregnation ratio is 4.5:1. Further increasing the impregnation ratio, the existing micropores expanded into mesopores, but new micropores almost no longer appeared, which reduced the BET surface area [13,14]. Therefore, 3:1 is the most suitable impregnation ratio, it results in the highest surface area and total pore volume.

Table 1 shows that when the impregnation ratio increases from 3:1 to 5:1, yields for AC decrease. It was mainly because of KOH promoted the dehydrating effect and the formation of cross-links during the heat treatment, which lead to some volatile matter produced [15]. However, the yields increase with continuing increase of the impregnation ratio. It was mainly because of too much KOH may plug pores of AC and prevent volatiles through pore channel.

Fig. 1 shows the nitrogen adsorption–desorption isotherms of AC. Similar trend can be observed in all the curve of AC. These N_2 adsorption isotherms shows type I characteristics which indicated their microporous features [16]. Fig.2 plotts the corresponding pore size distribution curves of AC. As for AC, harp peaks are in the range of pore diameter less than 2 nm which confirmed the primary pore size of AC was in the microspore range.

The effect of activation temperature

As seen from Table 1, Figs. 3 and 4, the N_2 uptake increases with the increasing of activation temperature, and reaches the maximum at 800 °C. A further increase of the activation temperature results in some decrease in the N_2 uptake. It is similar with the trend of total pore volume. And the yields decrease with increase of the activation temperature. These were mainly because of C-KOH reaction resulted in pore formation and carbon atom consumption of AC. While the pore development of carbon need the appropriate temperature, a higher temperature would result in excessive activation reactions that caused adverse effects on the development of internal pores. Then some micropores, which account for the large specific surface area, could be converted to mesopores due to over burn-off and resulted in the reduction of yield [17,18].

The effect of activation time

As seen from Table 1, Figs. 5 and 6, the N_2 uptake increases with increasing activation time up to 1.5 h and decreases thereafter. It is similar with the trend of total pore volume. In shorter activation time, pyrolysis polygeneration of hemp stems did not have enough time to promote the development of pores, thence led to low adsorption capacity. While too long activation time may cause over-activation, accelerating surface erosion, which transferring micropores to macropores or mesopores [19]. At the same time, the yields decrease with the increase of activation time attributed to the deeper burn-off degree. In addition, the steep rise and high N_2 uptake of the initial part of the N_2 adsorption–desorption isotherms and almost no hysteresis was found indicated that AC had a large number of micropores, but had few mesopores and macropores [20].

To sum up, the optimal conditions of preparing AC(AC1) are: an impregnation ratio of 4.5:1 (KOH/char), an activation temperature of 800 °C and an activation time of 1.5 h.

Table 1
Pore structure characteristic of hemp stems-based activated carbon.

Impregnation ratio (KOH/char)	Activation temperature (°C)	Activation time (h)	S_{BET} ($m^2 \cdot g^{-1}$)	V_{Total} ($cm^3 \cdot g^{-1}$)	V_{Micro} ($cm^3 \cdot g^{-1}$)	V_{Micro}/V_{Total} (%)	Dp (nm)	Yield (%)
3:1	800	1	1849	0.89	0.64	71.91	2.48	68.77
3.5:1	800	1	2010	0.98	0.80	81.63	2.25	64.33
4:1	800	1	2104	1.04	0.90	86.54	2.19	60.21
4.5:1	800	1	2312	1.21	1.05	86.78	2.15	58.46
5:1	800	1	2219	1.12	0.93	83.04	2.24	56.64
5.5:1	800	1	2171	1.09	0.85	77.98	2.39	58.22
6:1	800	1	2158	1.06	0.82	77.36	2.40	60.34
4.5:1	700	1	2029	0.84	0.69	82.14	2.00	62.50
4.5:1	750	1	2182	1.07	0.90	84.11	2.09	61.93
4.5:1	850	1	2250	1.16	0.97	83.62	2.43	56.39
4.5:1	900	1	2188	1.09	0.89	81.65	2.64	50.63
4.5:1	800	0.5	2066	1.02	0.82	80.39	2.24	66.30
4.5:1	800	1.5	2388	1.27	1.13	88.98	2.06	58.13
4.5:1	800	2	2146	1.13	0.98	86.73	2.17	56.96
4.5:1	800	2.5	2042	1.00	0.85	85.00	2.12	54.33

S_{BET}: BET specific surface area; V_{Total}: total pore volume; V_{Micro}: micropore volume; Dp: average pore diameter.

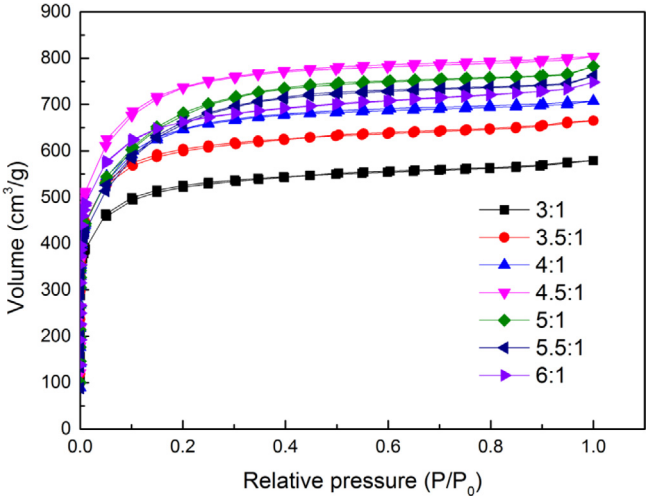

Fig. 1. Nitrogen adsorption–desorption isotherms for AC with different impregnation ratio (activation temperature is 800 °C, activation time is 1 h).

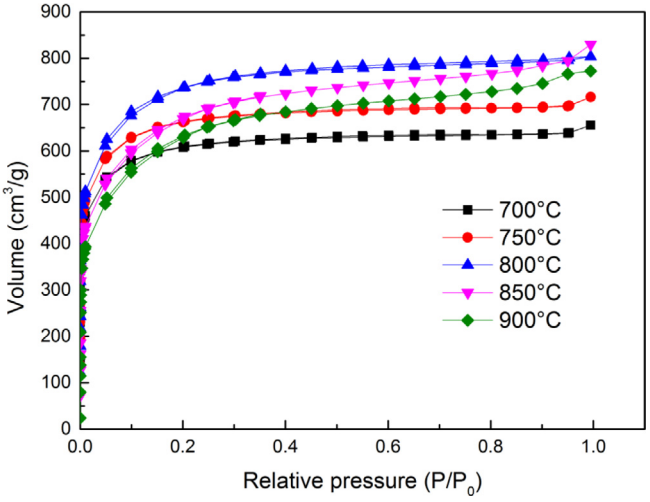

Fig. 3. Nitrogen adsorption–desorption isotherms for AC with different activation temperature (impregnation ratio is 4.5:1, activation time is 1 h).

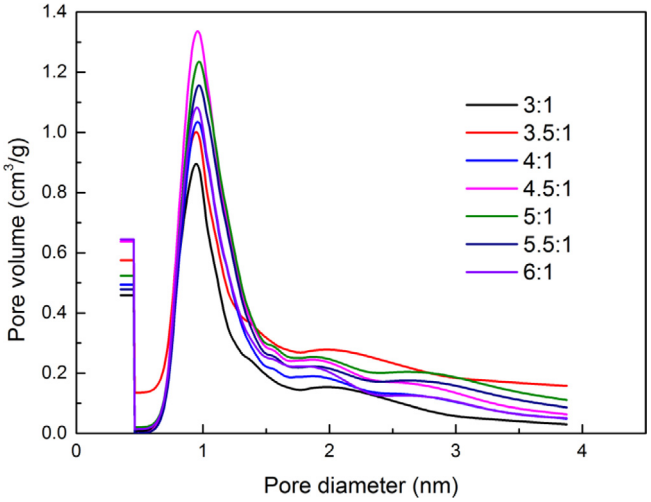

Fig. 2. Pore size distribution of AC with different impregnation ratio (activation temperature is 800 °C, activation time is 1 h).

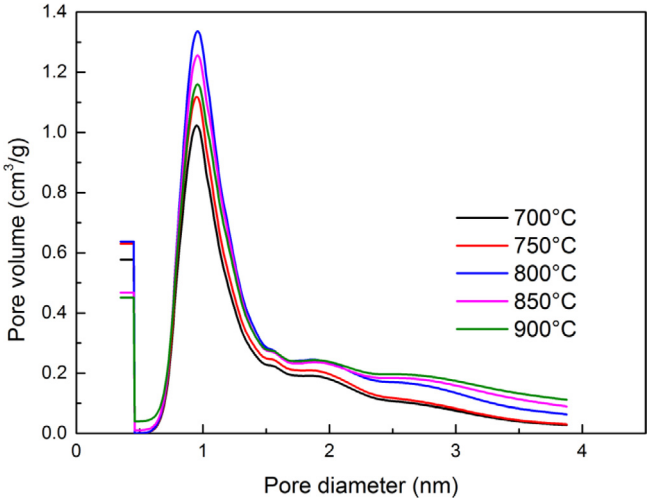

Fig. 4. Pore size distribution of AC with different activation temperature (impregnation ratio is 4.5:1, activation time is 1 h).

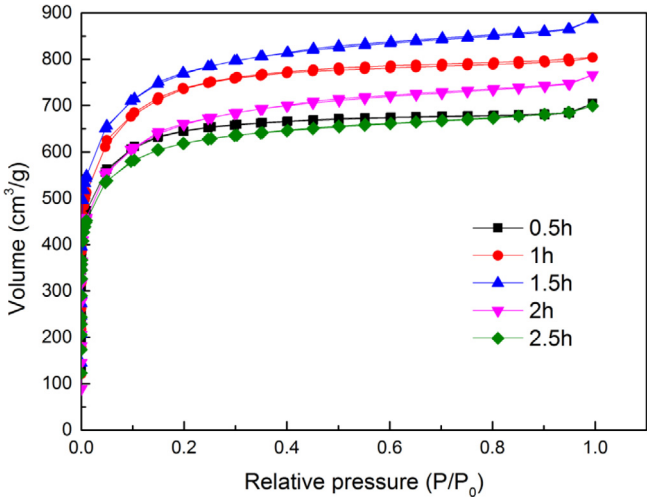

Fig. 5. Nitrogen adsorption–desorption isotherms for AC with different activation time (impregnation ratio is 4.5:1, activation temperature is 800 °C).

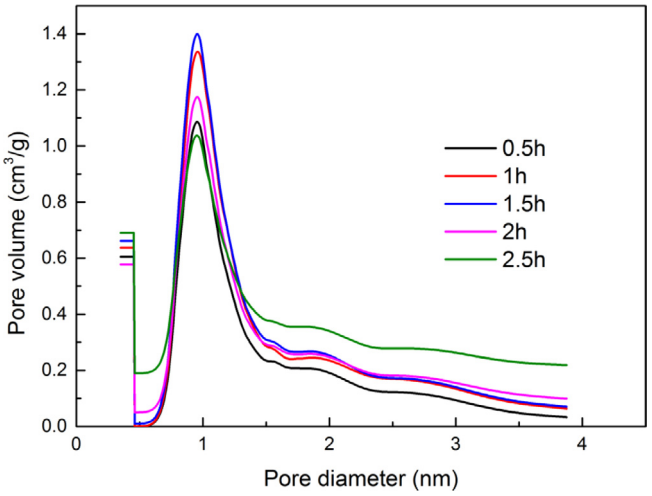

Fig. 6. Pore size distribution of AC with different activation time (impregnation ratio is 4.5:1, activation temperature is 800 °C).

FITR spectrum analysis

The 4000–400 cm^{-1} infrared spectral region of hemp stems, char and AC1 prepared by KOH activation at the optimal conditions are shown in Fig. 7. All spectra exhibit a wide band at 3200–3600 cm^{-1} with a maximum at 3420 cm^{-1}, which should correspond to the O–H stretching mode of hydroxyl groups and adsorbed water. A weak band at 604 cm^{-1} also appears in the spectra was most probably due to the out-of-plane deformation mode of O–H [21].

The FTIR spectra of hemp stems shows an obvious band at around 2920 cm^{-1} due to the C–H stretching in methyl and methylene groups, and a series of peaks present between 1460 and 1240 cm^{-1}, especially three major shoulder peaks at 1375, 1329 and 1244 cm^{-1}, respectively. The peak at 1375 cm^{-1} can be attributed to the in-plane symmetric deformation vibration of -CH_3 in lignin, and the peak at 1329 cm^{-1} is attributed to the inplane bending vibrations of O–H or stretching of C-O in cellulose, and the peak at 1244 cm^{-1} corresponds to the asymmetric stretching of =C—O—C connected with aryl groups in lignin [22]. It could be clearly seen that peaks corresponded to the structures of cellulose and lignin in hemp stems did not present in the spectra of hemp stems after carbonization or activation, which revealed the damage of organic compounds in hemp stems [23].

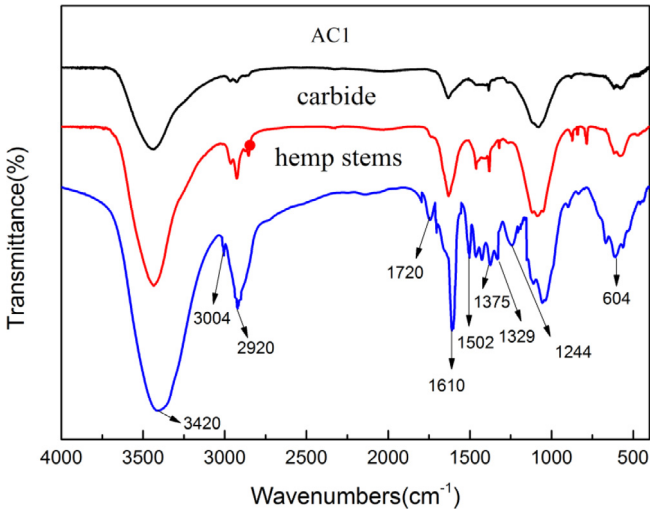

Fig. 7. FTIR spectra of different stages of preparation of AC.

For the char, the band at 3004 cm^{-1} corresponds to C–H in benzene rings and the band at 1502 cm^{-1} associates with benzene skeleton disappears, and the intensity of the band at 1610 cm^{-1} is ascribed to benzene skeleton decreased. The peak at 1720 cm^{-1} is identified as carboxylic groups disappeared, indicating they were oxidized to release CO and CO_2 and the multiplet in the 1300–900 cm^{-1} interval was ascribed to the ethers between rings, C=O in phenol, benzyl hydroxyl and other groups disappeared [24,25]. It could be clearly seen that carbonization changed the structure of hemp stems. The methylene bridge and ether bridge linking the benzene rings broke promoted benzene rings approached each other and appeared more polysubstitution. It could be seen that carbon network structure expanded after carbonization.

For the AC1 prepared by KOH activation at the optimal conditions, the predominant peaks weaken and some peaks vanish. The intensity of the peaks related to the hydroxyl (3430 cm^{-1}) and absorbed water (1628 cm^{-1}) significantly diminish corresponded to hydrophilic groups remarkably decreased. The peak is identified as carboxylic groups at 1720 cm^{-1} was ambiguous, indicating a further oxidation process to evolve CO and CO_2 [26]. All these characters indicated that KOH-impregnated char transformed to amorphous carbon. Methylene and oxygen-containing functional groups had a great reduction after activation.

TG-MS analysis

The thermogravimetric curve and differential thermogravimetric curve during pyrolysis of hemp stems and KOH-impregnated char at the heating rate of 10 °C/min are presented in Fig.8.

A weight loss of about 81.08% in 1000 °C is observed for hemp stems and the process can be divided into three steps: The first stage (3.45% weight loss) is mainly because of moisture evaporation at the temperature of about 110 °C. In the second stage weight loss has a great reduction between 200 and 375 °C. It is probably attributed to the hemicellulose decomposition. The maximum weight loss rate appears at 346 °C might be due to the maximum decomposition rate of the cellulose [27]. During the second stage about 65.91% of the total weight significantly diminishs. The last stage (375–1000 °C) in pyrolysis is the further cracking process of hemp stems residues due to lignin decomposition.

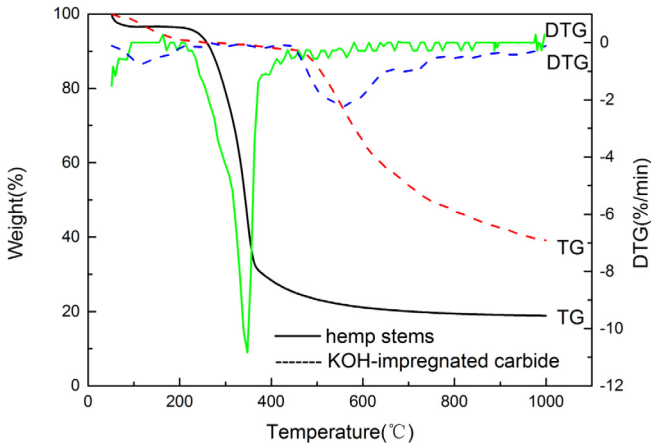

Fig. 8. TG and DTG curves for hemp stems and KOH-impregnated char.

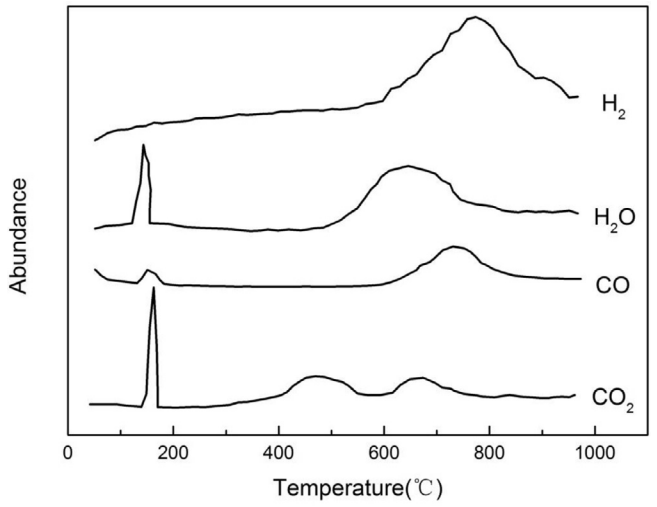

Fig. 9. MS responses of evolved gases in TG-MS analysis of KOH-impregnated char.

Compared with hemp stems, KOH-impregnated char had undergone a carbonization process at 500 °C, therefore it had the less weight loss at the same temperature. However, KOH-impregnated char has a remarkable weight loss of about 6.2% in 160–200 °C, which was attributed to the release of H_2O and CO_2 in 160–200 °C. And there is no obvious strong peak of H_2O appears at about 100 °C indicates a part of KOH attached on the char was converted to $KHCO_3$ by absorbing surrounding H_2O and CO_2. When the temperature reached around 200 °C, $KHCO_3$ is rapidly decomposed, which coincided with the increase of weight loss due to the generation of H_2O and CO_2 [28].

As shown in Fig. 9, the H_2 begins to evolve at temperature of 580 °C and reaches the maximum at about 774 °C for the latter, it can be inferred that probable reactions between KOH and char proceed are as below:

$$4KOH + C \rightarrow K_2CO_3 + K_2O + 2H_2 \quad (1)$$

The H_2O begins to evolve at temperature of 120 °C can be due to moisture evaporation. It appears again when the temperature rises above 500 °C can be attributed to the transforming of dehydrated KOH into K_2O [29].

$$2KOH \rightarrow K_2O + H_2O \quad (2)$$

The CO spectra in Fig. 9 exhibits the major feature at about 760 °C, which can be either come from the reaction between the evolved H_2O and carbon or the reaction of intermediate potassium oxide species, such as K_2CO_3 or K_2O with carbon [30].

$$C + H_2O \rightarrow CO + H_2 \quad (3)$$

$$K_2CO_3 + 2C \rightarrow 2K + 3C \quad (4)$$

$$K_2O + C \rightarrow 2K + CO \quad (5)$$

The CO_2 spectra exhibits a peak around 160 °C, which is attributed to the decomposition of carboxylic acid groups. Then another peak appears around 760 °C is mainly because of a significant contribution from the decomposition of the potassium carbonate product [31].

$$K_2CO_3 \rightarrow K_2O + CO_2 \quad (6)$$

Conclusions

The optimal conditions of preparing super activated carbon based on hemp stems are: an impregnation ratio of 4.5:1 (KOH/char), an activation temperature of 800 °C and an activation time of 1.5 h. The characterization of AC is as follows: The specific surface area is high up to 2388 $m^2 \cdot g^{-1}$, the total pore volume is 1.27 $cm^3 \cdot g^{-1}$ and the average pore diameter is 2.06 nm. It can be seen that the hemp stems-based activated carbon by KOH activation has high specific surface area, well-developed pore structure and evident microporous features, which can be contributed to either comprehensive utilization and sustainable development of hemp stem or environmental protection.

Reaction mechanism during the preparation of AC is as follows: reactions during the carbonization process primarily refer to scission reactions of methylene, oxidation of methylene and preliminary cyclization reactions. When the KOH-impregnated char is activated at 800 °C, reactions during the activation process are mainly related to polycyclic reactions, reactions between carbon and KOH, and reactions between intermediate potassium oxide species and carbon.

Acknowledgments

This study was supported by the National Natural Science Foundation of China (NSFC, No. 51572028), the National High Technology Research and Development Program of China (863 Program, No. 2015AA033905) and Beijing Training Project For The Leading Talents in S & T (No. 201424).

References

[1] Hirunpraditkoon S, Tunthong N, Ruangchai A, Nuithitikul K. Adsorption capacities of activated carbons prepared from bamboo by KOH activation. Proc World Acad Sci Eng Technol 2011;78:711.
[2] Gao N, Li A, Quan C, Du L, Duan Y. TG–FTIR and Py–GC/MS analysis on pyrolysis and combustion of pine sawdust. J Anal Appl Pyrol 2013;100:26–32.
[3] Yahya MA, Al-Qodah Z, Ngah CWZ. Agricultural bio-waste materials as potential sustainable precursors used for activated carbon production: A review. Renew Sustain Energy Rev 2015;46:218–35.
[4] Kazemipour M, Ansari M, Tajrobehkar S, Majdzadeh M, Kermani HR. Removal of lead, cadmium, zinc, and copper from industrial wastewater by carbon developed from walnut, hazelnut, almond, pistachio shell, and apricot stone. J Hazard Mater 2008;150(2):322.
[5] Kumar A, Jena HM. Preparation and characterization of high surface area activated carbon from Fox nut (Euryale ferox) shell by chemical activation with H3PO4. Results Phys 2016;6:651–8.
[6] Yang R, Liu G, Xu X, Li M, Zhang J, Hao X. Surface texture, chemistry and adsorption properties of acid blue 9 of hemp (Cannabis sativa L.) bast-based activated carbon fibers prepared by phosphoric acid activation. Biomass Bioenergy 2011;35(1):437–45.
[7] Wu X, Hong X, Nan J, Luo Z, Zhang Q, Li L, et al. Electrochemical double-layer capacitor performance of novel carbons derived from SAPO zeolite templates. Microporous Mesoporous Mater 2012;160(160):25–31.
[8] Altenor S, Carene B, Emmanuel E, Lambert J, Ehrhardt JJ, Gaspard S. Adsorption studies of methylene blue and phenol onto vetiver roots activated carbon prepared by chemical activation. J Hazard Mater 2009;165(1–3):1029–39.

[9] Rosas JM, Bedia J, José Rodríguezmirasol A, Cordero T. Preparation of hemp-derived activated carbon monoliths. adsorption of water vapor. Ind Eng Chem Res 2008;47(4):1288–96.
[10] Basta AH, Fierro V, El-Saied H, Celzard A. 2-Steps KOH activation of rice straw: an efficient method for preparing high-performance activated carbons. Bioresour Technol 2009;100(17):3941–7.
[11] Yang R, Liu G, Li M, Zhang J, Hao X. Preparation and N2, CO2 and H2 adsorption of super activated carbon derived from biomass source hemp (Cannabis sativa L.) stem. Microporous Mesoporous Mater 2012;158:108–16.
[12] Zhang J, Shang T, Jin X, Gao J, Zhao Q. Study of chromium(vi) removal from aqueous solution using nitrogen-enriched activated carbon based bamboo processing residues. RSC Adv 2015;5(1):784–90.
[13] Li Y, Li Y, Li L, Shi X, Wang Z. Preparation and analysis of activated carbon from sewage sludge and corn stalk. Adv Powder Technol 2016;27(2):684–91.
[14] Nieto-Delgado C, Rangel-Mendez JR. Production of activated carbon from organic by-products from the alcoholic beverage industry: Surface area and hardness optimization by using the response surface methodology. Ind Crops Prod 2011;34(3):1528–37.
[15] Açıkyıldız M, Gürses A, Karaca S. Preparation and characterization of activated carbon from plant wastes with chemical activation. Microporous Mesoporous Mater 2014;198:45–9.
[16] Zhang J, Jin XJ, Gao JM, Zhang XD. Phenol adsorption on nitrogen-enriched activated carbon prepared from bamboo residues. Bioresources 2014;9(1):969–83.
[17] Yang T, Lua AC. Characteristics of activated carbons prepared from pistachio-nut shells by potassium hydroxide activation. Microporous Mesoporous Mater 2003;63(03):113–24.
[18] Karagöz S. Adsorption of methylene blue from aqueous solution on activated carbon produced from soybean oil cake by KOH activation. Bioresources 2012;7(3):3175–87.
[19] Chen D, Chen X, Sun J, Zheng Z, Fu K. Pyrolysis polygeneration of pine nut shell: Quality of pyrolysis products and study on the preparation of activated carbon from biochar. Bioresour Technol 2016;216:629–36.
[20] Zhang F, Ma H, Chen J, Li GD, Zhang Y, Chen JS. Preparation and gas storage of high surface area microporous carbon derived from biomass source cornstalks. Bioresour Technol 2008;99(11):4803–8.
[21] Guo Y, Rockstraw DA. Physical and chemical properties of carbons synthesized from xylan, cellulose, and Kraft lignin by H_3PO_4 activation. Carbon 2006;44(8):1464–75.
[22] Fierro V, Torné-Fernández V, Celzard A. Kraft lignin as a precursor for microporous activated carbons prepared by impregnation with ortho-phosphoric acid: Synthesis and textural characterisation. Microporous Mesoporous Mater 2006;92(1–3):243–50.
[23] Yong C, Chang JM, Wang WL, Li B, Ren XY. Preparation of activated carbon using bio-oil phenol-formaldehyde resin. Bioresources 2015;10(3).
[24] Kirtania K, Tanner J, Kabir KB, Rajendran S, Bhattacharya S. In situ synchrotron IR study relating temperature and heating rate to surface functional group changes in biomass. Bioresour Technol 2014;151(1):36–42.
[25] Sreńscek-Nazzal J, Kamińska W, Michalkiewicz B, Koren ZC. Production, characterization and methane storage potential of KOH-activated carbon from sugarcane molasses. Ind Crops Prod 2013;47:153–9.
[26] Moniruzzaman M, Ono T. Separation and characterization of cellulose fibers from cypress wood treated with ionic liquid prior to laccase treatment. Bioresour Technol 2013;127(1):132–7.
[27] Wongsiriamnuay T, Tippayawong N. Non-isothermal pyrolysis characteristics of giant sensitive plants using thermogravimetric analysis. Bioresour Technol 2010;101(14):5638–44.
[28] Huang Y, Ma E, Zhao G. Thermal and structure analysis on reaction mechanisms during the preparation of activated carbon fibers by KOH activation from liquefied wood-based fibers. Ind Crops Prod 2015;69:447–55.
[29] Lozano-Castelló D, Calo JM, Cazorla-Amorós D, Linares-Solano A. Carbon activation with KOH as explored by temperature programmed techniques, and the effects of hydrogen. Carbon 2007;45(13):2529–36.
[30] Byamba-Ochir N, Shim WG, Balathanigaimani MS, Moon H. Highly porous activated carbons prepared from carbon rich Mongolian anthracite by direct NaOH activation. Appl Surf Sci 2016;379:331–7.
[31] Wang J, Kaskel S. KOH activation of carbon-based materials for energy storage. J Mater Chem 2012;22(45):23710.